JOURNAL OF MATERIALS SCIENCE **36** (2001) 937–941

Precipitation of α-Al(Fe,Mn)Si from the melt

J. E. TIBBALLS
Centre for Materials Science, University of Oslo, Forskningsparken, N-0349 Oslo, Norway; Senter for Industriforskning, Forskningsveien 1, N-0314 Oslo, Norway
E-mail: john.tibballs@fys.uio.no

J. A. HORST, C. J. SIMENSEN
Senter for Industriforskning, Forskningsveien 1, N-0314 Oslo, Norway

The cubic and hexagonal α-Al(Fe,Mn)Si phases have been precipitated slowly and equilibrated at 630°C from a series of melts with approximately 4 wt% transition metal and 7.5 wt% Si in which the Fe : Mn ratio has been varied from 30 : 1 to 1 : 10. Chemical analyses of the phases, and of the microstructure that formed on solidification of the residual melt, show that the total transition metal concentration in the mixed phase is less than in the almost stoichiometric compositions found for the end-member ternary α_c-AlMnSi produced previously under similar conditions. This is interpreted as evidence for a stabilising effect of vacancies which counters any destabilisation of the electronic structure arising from the second transition metal. The residual melt composition also exhibits a marked reduction in the total transition metal concentration that is further evidence of the enhanced stability of the mixed phase. The consequence for both liquidus and solvus precipitation reactions in dilute alloys is that the transition-metal enrichment necessary for precipitation is as low as 60% of that estimated from Phillips and Varley [1] who interpolate linearly between the end-member solubilities.

1. Introduction

The α-phase in the Al-Fe-Mn-Si alloy system is an important constituent of many aluminium and magnesium alloys. It forms both by interdendritic precipitation on solidification and by heterogeneous nucleation and growth in supersaturated grains when the alloy is annealed. The metallurgical quality of AA 3XXX canstock and related alloys including AA 4XX casting alloys requires control of the volume fraction and size distribution of the α-phase which are factors governing both strength and recrystallization characteristics.

Early phase diagrams for the Al-Fe-Mn-Si system [1, 2] showed a single α-phase, but it is now known to exist in two crystallographic modifications: α_c, a cubic structure with a body-centred arrangement of two-shell Mackay icosahedra [3, 4], and α_h an hexagonal lattice of distorted Mackay icosahedra [5]. The cubic structure is the stable form for the ternary phase α-AlMnSi and for iron concentrations up to Fe : Mn ratios of 9 : 1 [6]. The hexagonal form is restricted to almost pure α-AlFeSi with as little as 0.15 at.% Mn in an alloy reported to suppress its occurrence in castings cooled at a rate of 0.75 K/sec [7].

In a study [8] of the substitution of Al and Si in the ternary phase α_c-AlMnSi, the phase was precipitated from melts with varying silicon contents and equilibrated slightly above the temperature for the initial solidification of face-centred cubic aluminium. Chemical analyses of the microstructure determined the concentrations of the liquid and α-phase in two-phase equilibrium. Extraction of α-phase crystals in that study enabled both calorimetric [9] and crystallographic [8] investigations to provide data for the thermodynamic modelling of the ternary phase [10].

In order to obtain more information on which to base a thermodynamic description of the Fe-containing α-phases, the methods developed in [8] have been applied to Al-Fe-Mn-Si alloys with varying Fe : Mn ratios.

2. Experimental method

Alloy compositions were selected as shown in Table I from an examination of quaternary phase diagrams [1, 2]. The criteria, chosen so that the α-phase could be extracted, were:

i) α-Al(Fe,Mn)Si be the primary solidifying phase;
ii) the secondary phase be the f.c.c. solution of Fe, Mn and Si in aluminium;
iii) the yield of α-phase be maximal for each Fe : Mn ratio;
iv) the full range of Fe : Mn ratios be sampled.

The alloys were prepared as approximately 50 g ingots from 99.993% Al, 99.95% Mn, 99.99% Fe and semiconductor grade Si in $A1_20_3$ crucibles sealed in quartz glass ampoules under a 1/4 bar atmosphere of argon. The furnace-temperature cycle (controlled by a thermocouple placed inside the ceramic baffle which held the ampoule) was programmed to heat to 950 °C and hold for 12 hours. After cooling to T_a and holding

for 5 hours, the furnace was cooled over 20 hours to T_b at which temperature it was held for 30 to 40 hours. The ampoule was then removed directly to a cold-water bath and broken within 10 seconds.

Analyses were performed on polished sections with a CAMECA electron microprobe in wavelength-dispersive mode. The analysis was calibrated against samples from the previous study [8] which had been checked by wet-chemical analysis. The analyses of the α-phase particles and of the solidified residual melt are included in Table I. The residual melt composition was found by scanning the electron beam over four $50 \times 50\ \mu m^2$ regions of the fine solidification microstructure. The uncertainties quoted in Table I reflect the standard deviation of the four measurements. Some precipitates were extracted from each ingot by dissolving the aluminium phase in butanol [11] and examined in the scanning electron microscope. X-ray diffraction intensities were measured using Cu K_α radiation on powders produced by crushing extracted particles after first removing the finely dispersed interdendritic precipitates by sieving. Silicon powder (NBS Standard Reference Material 640b) was added as a standard. The lattice parameters, obtained by Riley-Nelson analysis of the d-values for reflections out to $h^2 + k^2 + l^2 = 230$, are included in Table II together with densities obtained by pychnometer measurement of 250 mg of large crystals from each extraction. Air bubbles tended to form on the crystals so they were treated with ultrasound in the pychnometer; a treatment which caused the crystals from alloys 2, 3 and 5 to fracture. For the α-AlMnSi sample (from alloy 7) the density was determined by weighing in air and in distilled water to which detergent had been added at a concentration of $1:10^4$ to suppress bubble retention.

3. Results and discussion

3.1. Equilibrium reaction

The results of analyses of the phases are related to the ternary phase diagrams in Fig. 1. The primary precipitates, which formed and grew from the liquid to dimensions from 0.5 to 2 mm as the temperature was lowered to T_b, were found at the base of the ingots. In alloy 1, the primary precipitates consisted of a core of α_h-phase encapsulated in β_m-AlFeSi from a second, peritectic reaction. X-ray diffraction patterns from large particles extracted from alloy 1 exhibited distinct peaks from the monoclinic β_m-AlFeSi phase.

The microstructure of the solidified residual melts consisted of finely dispersed phases in regions between dendrite arms which had spacings of 7–25 μm. In the manganese-rich alloys, α-phase and silicon dominated, but in alloys 1 and 2, β_m-AlFeSi and silicon were found. In all cases, the occurrence of silicon shows that the interdendritic melt composition reached the quaternary eutectic;

$$\text{Liquid} \rightarrow \text{f.c.c. Al(Fe,Mn,Si)} + \text{Si} + \alpha_c(\text{or } \beta_m)$$

The question remains as to which stage of solidification is represented by the averaged composition

TABLE I Analyses of precipitates and estimates of the melt concentration Alloys M_1 and M_2 from [ref. 7] are included for comparison (n.q. = no analysis quoted)

Alloy ID	Holding Temp. [°C] T_a	T_b	Initial mixture Fe	Mn	Si	Composition [wt%] (std.dev.) Residual melt Fe	Mn	Si	α-phases (h = hexagonal; c = cubic) β-phase (m = monoclinic) Fe	Mn	Si	
M_1			2.5	0.2	6.0	n.q	n.q	n.q	30.7	1.3	n.q	h
M_2			2.5	0.3	6.0	n.q	n.q	n.q	25.2	4.8	n.q.	c
1		620	3.5		8.0	1.4(4)		8.3(1.4)	32.8(0.3)		9.4(0.3)	h
									24.9(0.6)		15.4(0.3)	m
2	680	630	3.0	0.1	7.5	1.3(3)	0.07(3)	8.0(1.0)	29.9(0.3)	0.95(0.1)	9.8(0.3)	h
4	690	630	3.0	1.0	7.5	0.9(2)	0.16(3)	8.3(0.3)	20.8(0.2)	8.6(0.2)	8.3(0.5)	c
3	710	630	1.9	1.9	7.5	0.4(1)	0.35(3)	8.6(0.2)	13.1(0.2)	14.4(0.3)	9.2(0.3)	c
5	720	630	1.0	3.0	7.5	0.14(2)	0.49(5)	9.1(0.3)	6.1(0.2)	21.0(0.3)	10.l(0.3)	c
6	730	630	0.4	3.6	7.5	0.04(1)	0.69(7)	7.4(1.8)	2.0(0.1)	28.3(0.2)	10.7(0.2)	c
7#	730	650		4.4	7.1		0.80(8)	6.6(0.9)		29.5(0.3)	11.0(0.3)	c

#Data from ref. 8 casting no.3.

TABLE II X-ray diffraction and density data for α-Al(Fe,Mn)Si phases

Source of α-phase (alloy no.)	Lattice parameter [nm]	Density [$kg \cdot m^{-3}$]	Number of atoms in unit cell Al	Si	Mn	Fe	Total
1	1.2433(6)	not	166	26		45	237
hexagonal	2.6149(5)	measured					(ideal [5])
2	1.2404(14)	3640 ± 20	168.5	26.2	1.3	41.0	237 ± 1.3
hexagonal	2.621(3)						
4	1.2588(2)	3620 ± 20	100.5	12.9	6.8	16.2	136.4 ± 0.8
3	1.2609(3)	3520 ± 20	99.5	13.9	11.1	10.0	134.5 ± 0.8
5	1.2650(2)	3520 ± 20	99.1	15.4	16.4	4.6	135.5 ± 0.8
6	1.2657(2)	3540 ± 20	94.7	16.4	22.3	1.5	134.9 ± 0.8
7	1.2658(1)	3630 ± 20	97.3	17.5	24.0	0	138.8 ± 0.8

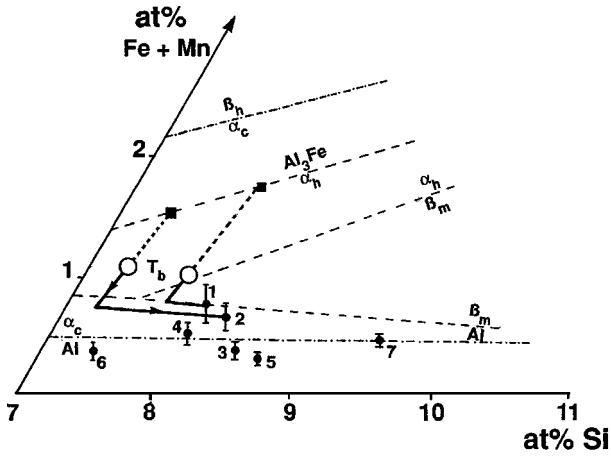

Figure 1 Portion of the Al-Fe-Mn-Si liquidus diagram projected down the Fe-Mn edge. The dashed lines mark phase boundaries for the ternary Al-Mn-Si alloy system; the dot-dash lines are for ternary Al-Fe-Si. For alloys 1 and 2, the heavy lines illustrate the melt composition in equilibrium with the large precipitates during slow cooling (dashed) from the alloy composition (filled squares) to the intended holding composition (open circles labelled Tb), and during rapid cooling (full line). For the remaining alloys, the melts started with compositions near alloy 2 and ended at the residual melt compositions denoted by the numbered filled circles.

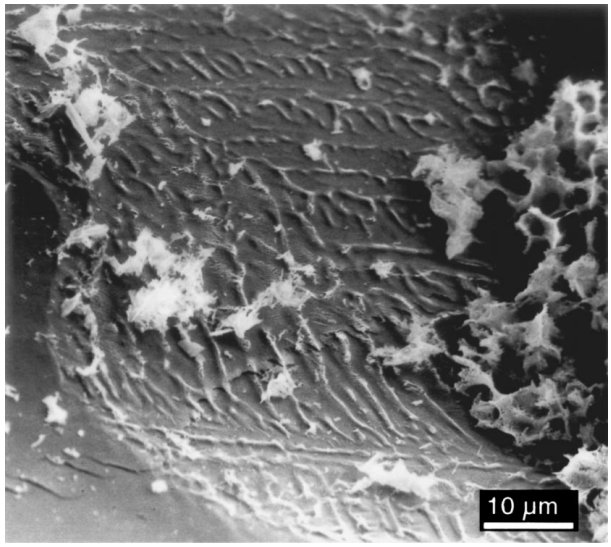

Figure 2 The surface of a large particle extracted from alloy 1 showing interdendritic β_m-phase growing out of a peritectic layer of the same phase. The filligree is the remains of other interdendritic precipitation that formed during quenching, seen here after dissolving the aluminium dendrites.

(Table I) of the fine-structured residual melt. Analysis of the surface of particles extracted from alloy 1 revealed a layer of β_m-AlFeSi with ridges approx. 7 μm apart (Fig. 2). The ridges result from the nucleation of the dendrites of f.c.c. Al(Fe,Mn,Si) (dissolved on extraction) coupled with growth of the β_m-phase into the melt during cooling at approx 400°C/s. The melt concentration has crossed the liquidus surface for peritectic precipitation of β_m-AlFeSi and has begun moving along the eutectic valley L $\rightarrow$ f.c.c. + β_m. From this time, the large particles grow no larger. The averaged residual melt composition therefore represents a point in this valley in the direction of the quaternary eutectic from its intersection with line representing the precipitation of the larger particles.

On quenching alloy 2, the melt concentration has crossed the remainder of the Liq $\rightarrow$ Liq + α_h surface and moved down the eutectic valley first for L $\rightarrow$ f.c.c. + α_h and then L $\rightarrow$ f.c.c. + β_m. This path is emphasised in Fig. 1, in which the residual-melt concentrations are superimposed on the liquidus boundaries for the Al-Fe-Si and Al-Mn-Si systems from [1]. For the remaining alloys, the residual melt concentrations have crossed the Liq $\rightarrow$ Liq + α_c surface and moved down the Liq $\rightarrow$ Liq + f.c.c. + α_c eutectic valley.

For the ternary alloys 1 (Al-Fe-Si) and 7 (Al-Mn-Si), the measured residual melt compositions lie on the eutectic boundaries [1] for simultaneous precipitation of the fc.c. solid solution and the β_m- and α_c-phase, respectively. The residual melt compositions of the quaternary alloys can similarly be taken represent the eutectic boundary at a silicon concentration slightly greater than that for which f.c.c. aluminium first precipitates. Since this boundary is almost parallel to the Si axis, the measured residual melt concentrations of Fe and Mn lie with in 0.05 wt% of the Fe and Mn concentrations for the three-phase equilibria which mark the end of primary precipitation:

$$\text{Liq} \rightarrow \text{Liq} + \alpha_c \text{ (or } \alpha_h \text{ or } \beta_m)$$

The silicon concentration at this equilibrium was again estimated by extending the lever construction from the precipitate concentration, through the composition of the intial melt to the eutectic boundary.

Since no segregation was observed between the surface or bulk of the large α-phase particles, the composition of the α-phase that enters into this equilibrium can be taken as that given in Table I.

The eutectic liquidus boundary for the quaternary system obtained in this way for approx. 7.5 at% Si is shown in Fig. 3. The melt concentration for the coupled precipitation of aluminium and the α- or β-phase from the liquid are significantly less than previously accepted [1]. Fig. 3 shows that, for Mn : Fe ratios

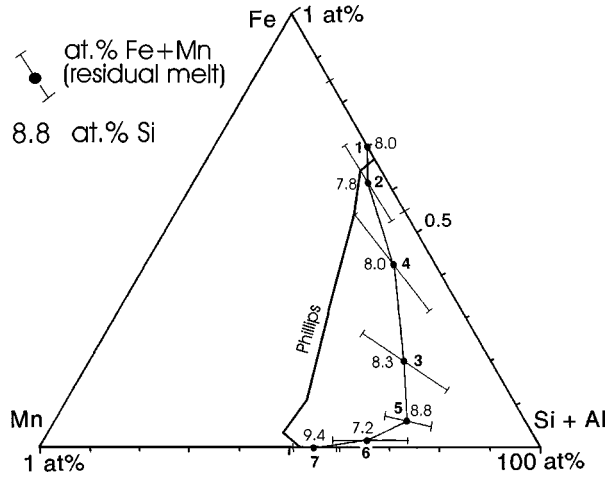

Figure 3 Projection of the Al-Fe-Mn-Si phase diagram down the Al-Si edge for concentrations greater than 99 at% Al + Si. Residual melt concentrations shown for each alloys demonstrate a strong deviation from the linear interpolation suggested by [1].

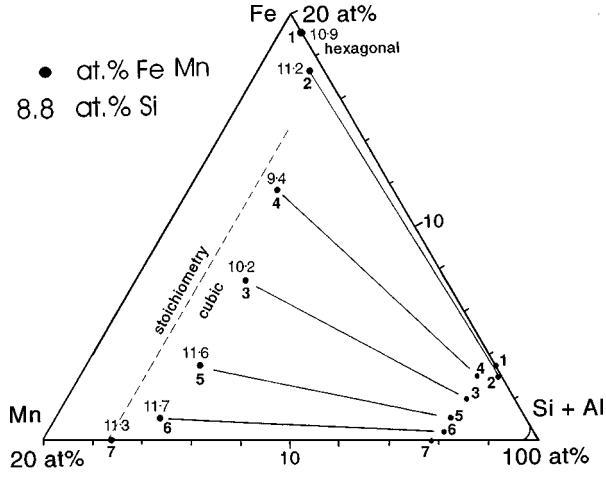

Figure 4 Projection of the Al-Fe-Mn-Si phase diagram down the Al-Si edge for concentrations greater than 80 at% Al + Si showing the compositions of large alpha phase particles in alloys 1 to 7. The numbered points at approximately 98 at% (Al + Si) represent the starting alloy compositions. The silicon concentrations are given in at.% for each phase.

of approximately 3 : 1, the maximum solubility of the transition metals in aluminium is 60% less than the solubility indicated in [1].

3.2. The α-phases

X-ray powder diffraction from the α-phase separated from alloys 1 and 2 shows the crystal structure to be the hexagonal variant α_h, while the remaining alloys had precipitated the cubic α_c-phase. The inclusion of approximately 1 wt% Mn in the α_h-phase from alloy 2 has reduced the total concentration of iron and manganese in the α_h-phase to 31–32 wt%, in the present case from 33 wt.% in the pure ternary α_h-AlFeSi phase. The silicon concentrations are higher than those reported previously [5, 7, 12] correlating with the higher silicon concentrations in the alloys. Nonetheless, the cell dimensions are larger than reported in other studies [5, 12] performed on samples with greater transition metal content. The density measurements (Table II) show that the increase in the numbers of silicon atoms per unit cell occurs by substitution for aluminium atoms, as also found in ternary α_c-AlMnSi [8].

The Fe : Mn dependence of the composition of the cubic α_c-phase (Fig. 4) shows a reduction in total transition metal (Fe + Mn) concentration when iron is added to ternary α_c-AlMnSi. While this follows the observed melt concentration in the equilibrium, it contradicts Mondolfo's [13] phase diagram indicating an increase in transition-metal content.* The measured densities and dimension and composition data (Table II) show the lowest (Fe + Mn) concentration (15.6 at%) in the α_c-phase to represent a deficit of 2.5 atoms per unit cell from full occupancy of the 24 atomic sites. Whether the vacancies stabilise the structure by compensating the extra valence electron supplied by iron, or through an additional entropy contribution due to disorder remains unclear. However, the ordering of four vacancies per unit cell, invoked [14] to relate the structure of the q-AlFeSi phase formed in the interdendritic regions of commercial alloys to the structure of α_c-Al(Fe,Mn)Si suggests that the entropy of disorder is of minor importance at solidification temperatures.

* NB! Mondolfo's projection from the aluminium corner on to the Al_3Fe-Al_6Mn-Si plane does not bear quantitative interpretation.

4. Conclusions

By precipitating, extracting and analysing the hexagonal and cubic α-Al(Fe,Mn)Si phases from slowly cooled melts with fixed transition-metal and silicon contents but varying the Fe : Mn ratios, phase diagram data for the liquidus surface of the quaternary alloy have been determined along the eutectic valley: Liq $\rightarrow$ Liq + α + Al(Fe,Mn,Si). The total transition metal content of the melt is markedly lower for the quaternary alloys than the respective end-member ternaries. A given alloy will, on solidification, precipitate more α-phase than expected from previously published phase diagrams.

For mixed Fe-Mn compositions of the α-phases, i.e., the quaternary extensions of the ternary phases, the total transition-metal content is up to 2.5 atoms less than the 24 Mn atoms per unit cell in the ternary cubic phase and the 45 Fe atoms in the hexagonal phase.

By focussing on the characteristics of the precipitating α-phases and the equilibria into which they enter, the study has provided, via thermodynamic evaluation [e.g., 10] of the alloy system, data on the stability of the two α-phases as a function of Fe : Mn ratio. The results contribute to the computation of the precipitation expected from dilute, wrought aluminium alloys of the AA 3XXX series as well as from casting alloys (AA 4XX series) with silicon contents more closely comparable with the alloys in the study. The same methodology also makes the data applicable to AS-series magnesium alloys.

Acknowledgements

Funding from the Norwegian Research Council and the financial support of Hydro Aluminium a.s. and Elkem Aluminium a.s. are gratefully acknowledged. The authors thank their colleagues T. Wahl and R. Kalland for their assistance in producing and preparing the alloy samples and T. -L. Rolfsen for the X-ray investigation.

References

1. H. W. L. PHILLIPS and P.C. VARLEY, *J. Inst. Metals* **69** (1943) 317.
2. G. PHRAGMEN, *ibid.* **77** (1950) 489.
3. M. COOPER and K. ROBINSON, *Acta Crystallogr.* **20** (1966) 614.
4. M. COOPER, *ibid.* **23** (1967) 1106.
5. R. N. CORBY and P. J. BLACK, *ibid.* **B33** (1977) 3468.
6. C. Y. SUN and L. A. MONDOLFO, *J. Inst. Metals* **95** (1967) 384.
7. D. MUNSON, *ibid.* **95** (1967) 217.
8. J. E. TIBBALLS, R. L. DAVIS and B. A. PARKER, *J. Mater. Sci.* **24** (1989) 2177.
9. K. REDFORD, J. E. TIBBALLS and R. MCPHERSON, *Thermochimica Acta* **158** (1990) 115.

10. Å. JANSSON and T. G. CHART, in Proceedings of the COST 507 Final Workshop, Vaal, The Netherlands, March 1997 (European Commission DG XII, Luxembourg).
11. C. J. SIMENSEN, P. FARTUM and A. ANDERSEN, *Fresnius Z. Anal. Chem.* **319** (1984) 286.
12. A. GRIGER, *Powder Diffraction* **2**(1) (1987) 31.
13. L. A. MONDOLFO, "Aluminium Alloys Structure and Properties," (Butterworth, London, 1974) p. 662.
14. PING LIU, and G. W. DUNLOP, *J. Mater. Sci.* **23** (1988) 1419.

Received 24 November 1999
and accepted 3 July 2000